OPTICS

Anti-coalescence of bosons on a lossy beam splitter

Benjamin Vest,[1] Marie-Christine Dheur,[1] Éloïse Devaux,[2] Alexandre Baron,[3] Emmanuel Rousseau,[4] Jean-Paul Hugonin,[1] Jean-Jacques Greffet,[1] Gaétan Messin,[1] François Marquier[1]*

Two-boson interference, a fundamentally quantum effect, has been extensively studied with photons through the Hong-Ou-Mandel effect and observed with guided plasmons. Using two freely propagating surface plasmon polaritons (SPPs) interfering on a lossy beam splitter, we show that the presence of loss enables us to modify the reflection and transmission factors of the beam splitter, thus revealing quantum interference paths that do not exist in a lossless configuration. We investigate the two-plasmon interference on beam splitters with different sets of reflection and transmission factors. Through coincidence-detection measurements, we observe either coalescence or anti-coalescence of SPPs. The results show that losses can be viewed as a degree of freedom to control quantum processes.

Surface plasmon polaritons (SPPs) are collective oscillations of electrons that propagate along a metal-dielectric interface (*1*). Several groups have reproduced fundamental quantum optics experiments with such surface plasmons instead of photons, as both are bosons. Observations of single-plasmon states (*2*, *3*), wave-particle duality (*4*, *5*), preservation of entanglement of photons in plasmon-assisted transmission (*6*–*8*), and more recently, two-plasmon interference have been reported in a large variety of plasmonic circuits (*3*, *9*–*12*). The ability to generate pairs of indistinguishable single SPPs is an important requirement for potential quantum information applications (*13*–*15*).

When dealing with two indistinguishable particles, the correlations at the output of a beam splitter are associated to the bosonic or fermionic character of the particles (*16*); that is, to the symmetry of the two-particle state $|\Psi_{\rm spatial}\rangle = \frac{|a\rangle_1|b\rangle_2 \pm |b\rangle_1|a\rangle_2}{\sqrt{2}}$, where a and b are the output ports of the beam splitter and the numbers 1 and 2 label the particles. At first glance, the observation of coalescence appears to be a signature of the bosonic nature of SPPs or photons. However, it has been pointed out that anti-coalescence can be observed with photons when using particular input states (*17*, *18*). This behavior stems from the introduction of the polarization degrees of freedom in the wave function: The global photonic state $|\Psi_{\rm tot}\rangle = |\Psi_{\rm pol}\rangle \otimes |\Psi_{\rm spatial}\rangle$ remains symmetric, but both the polarization state $|\Psi_{\rm pol}\rangle$ and the spatial state $|\Psi_{\rm spatial}\rangle$ are antisymmetric. The polarization state is the entangled antisymmetric Bell state $|\Psi_{\rm pol}\rangle = \frac{|H\rangle_1|V\rangle_2 - |V\rangle_1|H\rangle_2}{\sqrt{2}}$, where H (resp. V) is the horizontal (resp. vertical) state of polarization. Hence, when a nonpolarizing beam splitter is illuminated with the global photonic state $|\Psi_{\rm tot}\rangle$ and if the detectors are not sensitive to the polarization, the setup operates only on the spatial part of the state and output correlations reveal anti-coalescence, similar to the fermionic case. This property has been used as a method of analyzing Bell states (*18*). These ideas have been further used to mimic fermions with bosons (*19*). We also note that anti-coalescence of photons has been observed when preparing photon pairs in specific input states of the device (*20*, *21*) or in the context of a quantum eraser experiment, which is also based on the interplay between the spatial state and the polarization state (*22*). In all these works, it was assumed that the beam splitter is unitary and, therefore, that the phase difference between the reflection and the transmission factor is ±90°.

As previously shown (*23*, *24*), it is possible to change this phase difference when considering losses in the beam splitter. Indeed, it is shown that the presence of losses (scattering or absorption on the beam splitter) relaxes constraints on the reflection and transmission factors, allowing the control of their relative phase. Barnett *et al.* (*23*) and Jeffers (*24*) predicted, in particular, novel effects, including coherent absorption of single-photon and N00N states (*25*, *26*). Although losses are detrimental for the observation of squeezed states, they can thus be seen as a degree of freedom in the design of plasmonic devices, revealing new quantum interference scenarios.

Here we report the observation of two-plasmon quantum interference between two freely propagating, nonguided SPPs interfering on lossy plasmonic beam splitters. We designed several plasmonic beam splitters with different sets of reflection and transmission factors that are used in a plasmonic version of the Hong-Ou-Mandel (HOM) experiment (*27*), in which the input state is a symmetric spatial state and has no internal degrees of freedom: The polarization of the SPPs is fixed. Depending on the plasmonic beam splitters, coincidence measurements lead either to a HOM-like dip—i.e., a signature of plasmon coalescence—or a HOM peak that we associate to plasmon anti-coalescence. In the latter case, the anti-coalescence is fundamentally related to the beam splitter itself, and to its phase properties (*28*). This effect is a reminder that the bosonic nature of particles, here surface plasmons, does not imply bunching at a beam splitter.

Our experimental setup is based on a source of photon pairs (Fig. 1). The photons of a given pair are sent to two photon-to-SPP converters, located at the surface of a plasmonic test platform. The photon number statistics are conserved when coupling the photonic modes to a plasmonic mode on such a device (*29*) so that pairs of incident single-photons are converted into two single SPPs. These SPPs freely propagate on the metallic surface toward the two input arms of a plasmonic beam splitter. After the beam splitter, the SPPs that reach the output of the platform are converted back to photons to be detected by single-photon counting modules (SPCMs).

The plasmonic platform consists of several elements that are etched on a 300-nm-thick gold film on top of a silica substrate, on a total 40-µm by 40-µm footprint (Fig. 2). The input channels of the plasmonic platform are made of two unidirectional launchers (designated L1 and L2). These asymmetric 11-groove gratings have been designed to efficiently couple a normally incident Gaussian mode into directional SPPs (*30*). The SPPs generated by each launcher then freely propagate and recombine on the surface plasmon beam splitter (SPBS). It is made of two identical grooves in the metallic surface (Fig. 2C), oriented at 45° with respect to the propagation direction

Table 1. Dimensions of the plasmonic platform samples under study, as measured by a scanning electron microscope (width *w* and metal gap *g*) and atomic force microscope (groove depth *h*). Variables *w*, *g*, and *h* are described in Fig. 2C. The fourth row reports expected values for the reflection and transmission factors *r* and *t* based on the numerical simulations of the target design. The last row reports estimations of the relative phase between the reflection and transmission coefficients after characterization. Numbers between parentheses are the target dimensions and relative phase of the devices, as designed by numerical simulations.

Variable	Sample I	Sample II
w (nm)	171 (180)	289 (320)
g (nm)	145 (140)	250 (280)
h (nm)	140 (120)	150 (140)
$\lvert r\rvert/\lvert t\rvert$	(0.42/0.42)	(0.5/0.48)
$2\phi_{rt}$	170° (180°)	10° (0°)

[1]Laboratoire Charles Fabry, Institut d'Optique, CNRS, Université Paris-Saclay, 91127 Palaiseau cedex, France. [2]Institut de Science et d'Ingénierie Supramoléculaire, CNRS, Université de Strasbourg, 67000 Strasbourg, France. [3]Centre de Recherche Paul Pascal, CNRS, 33600 Pessac, France. [4]Laboratoire Charles Coulomb, UMR CNRS-UM 5221, Université de Montpellier, 34095 Montpellier, France.
*Corresponding author. Email: francois.marquier@institutoptique.fr

of waves launched by L1 and L2. The succession of metal and air allows a scattering process that generates both a transmitted and a reflected SPP (*31*), but this also introduces losses. The complex reflection and transmission factors $r = |r|e^{i\phi_r}$ and $t = |t|e^{i\phi_t}$ of the SPBS are functions of the geometrical parameters of the SPBS (Fig. 2C). In particular, it is possible to control the phase difference $\phi_{rt} = \phi_t - \phi_r$. This phase control will affect the interferences. The SPPs then propagate toward two large out-coupling strip slits. They are decoupled into photons propagating in the glass substrate on the rear of the platform.

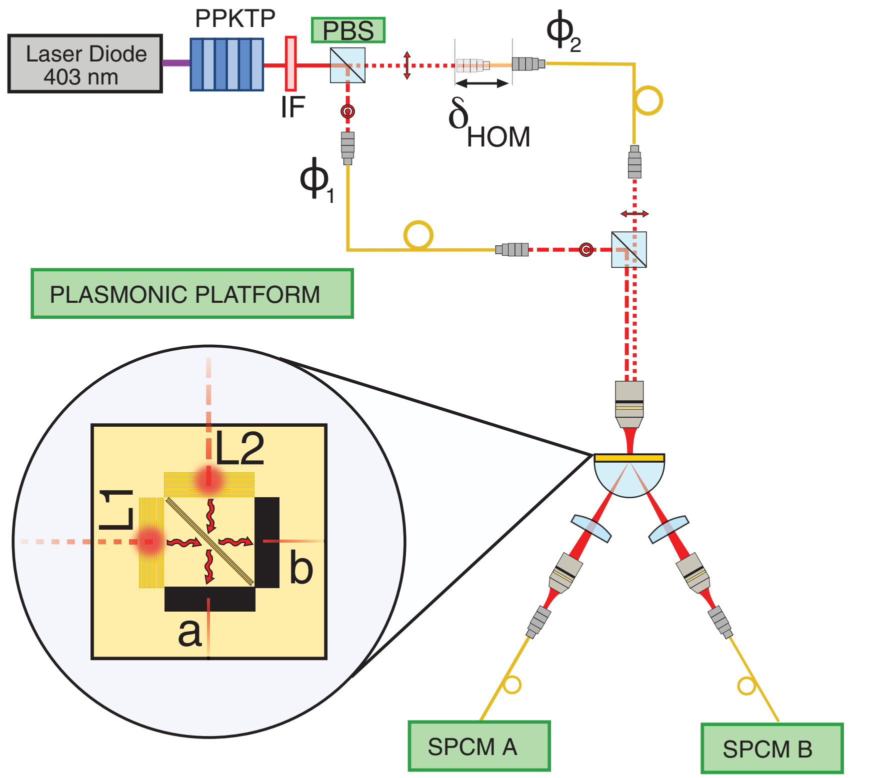

Fig. 1. Sketch of the experimental setup. A periodically poled potassium titanyl phosphate (PPKTP) crystal is pumped by a laser diode at 403 nm and delivers pairs of orthogonally polarized photons at 806 nm. An interference filter (IF) removes the remaining pump photons. The near-infrared photons are separated by a polarizing beam splitter (PBS) and injected in monomode fibers. The red dot within the circle and the red arrow represent the photon polarization after the PBS. They therefore excite the photonic modes Φ_1 or Φ_2, which are converted by the SPP launchers L1 and L2, respectively, into plasmonic modes on a plasmonic platform. One of the fiber collimator inputs is placed on a translation so that a delay δ_{HOM} between the two SPPs can be settled, changing the optical path of one of the photons after the PBS. The two single SPPs are recombined on a plasmonic beam splitter and finally out-coupled to photonic modes a and b. The light is transmitted form the substrate to the free space by a hemispherical lens before being collected by two 75 mm–focal length lenses at both output ports of the platform and is injected by two focusing objectives in multimode fibers. SPCMs A and B record detection counts from output modes a and b, respectively, and measure coincidences between the detectors.

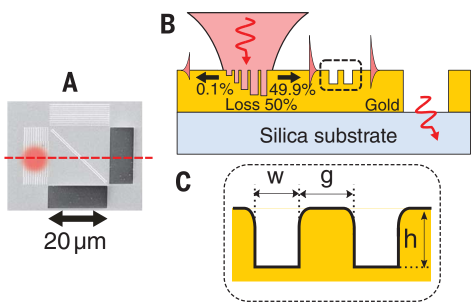

Fig. 2. Presentation of the plasmonic platform. (**A**) Scanning electron microscopy image of a plasmonic platform. The length and width of the grating grooves and outcoupling slits are 20 µm and 10 µm, respectively. The dotted red line represents the location of the cross section depicted in (B). The red spot represents an incident Gaussian beam on the SPP launcher. (**B**) Cross-sectional drawing of the device. On the left, the first structure is a photon-to-SPP coupler. When single photons (red arrow) reach the grating, single SPPs are launched unidirectionally toward the plasmonic beam splitter (SPBS) (grooved doublet enclosed by black dashed line). The remaining SPPs propagate to the large out-coupling slit. With an efficiency of about 50%, SPPs are converted back to photons in the silica substrate. (**C**) Close-up view of the SPBS. Dimensions of the SPBS are defined by three parameters: The groove width *w*, the metal gap between the grooves *g*, and the height of the groove *h*, which affect the reflection and transmission factors of the beam splitter.

For a lossless balanced beam splitter, energy conservation and unitary transformation of modes at the interface imposes $t = \pm ir$ and $|t| = |r| = \frac{1}{\sqrt{2}}$ so that the phase difference between r and t is $\phi_{rt} = \pm 90°$. When placed at the output of a Mach-Zehnder interferometer, the two outputs of the beam splitter deliver two sinusoidal interference signals that display a phase shift $2\phi_{rt} = \pm 180°$. It follows that a maximum on a channel corresponds to a minimum on the other channel, as expected from energy conservation arguments. The situation is different in our experiment; a single SPP is transmitted with probability $|t|^2$ and reflected with a probability $|r|^2$, but can be absorbed or scattered with a probability $1 - |t|^2 - |r|^2$. For a balanced SPBS, in the presence of losses, r and t are constrained by the following inequality (*13*)

$$|t \pm r|^2 \leq 1$$

where the equality holds only if there are no losses. The previous relation releases constraints on $2\phi_{rt}$. In other words, losses can here be considered as a new degree of freedom. It is therefore possible to design several beam splitters where the amplitudes of r and t and the relative phase ϕ_{rt} can be modified. As a direct consequence, interference fringes from both outputs of the SPBS can be found experiencing an arbitrary phase shift.

Controlling those properties of the SPBS strongly affects the detection of events by the two SPCMs. It has been shown (*23*) that the coincidence-detection probability, i.e., the probability for one particle pair to have its two particles emerging from separate outputs of the beam splitter, can be expressed as

$$P(1_a, 1_b) = |t|^4 + |r|^4 + 2\Re(t^2 r^2) I$$

where $2\Re(t^2r^2) = t^2 r^{*2} + t^{*2} r^2$, a and b label the output ports of the beam splitter, and I is an overlap integral between the two particles' wave packets. For nonoverlapping wave packets, $I = 0$, and the previous relation reduces to

$$P_{cl}(1_a, 1_b) = |t|^4 + |r|^4$$

The particles impinging on the SPBS behave like two independent classical particles, as indicated by the subscript cl. For an optimal overlap between the particles ($I = 1$), the coincidence probability can be written as

$$P_{qu}(1_a, 1_b) = |t^2 + r^2|^2 = P_{cl}(1_a, 1_b) + 2\Re(t^2 r^2)$$

where the subscript qu denotes the presence of the quantum interference term $2\Re(t^2r^2)$.

We now consider two cases. If $t = \pm ir$, the probability P_{qu} reaches zero. This is the same antibunching result that is obtained for a nonlossy beam splitter (15). This is the so-called HOM dip in the correlation function. If we now consider $t = \pm r$ with $|t| = |r| = \frac{1}{2}$, we get $P_{qu}(1_a, 1_b) = 2P_{cl}(1_a, 1_b)$. Here we expect a peak in the correlation function.

The plasmonic chips were designed by solving the electrodynamics equations with an in-house code based on the aperiodic Fourier modal method (32). Numerical simulations allowed us to find the geometrical dimensions of the beam splitter required for the two previous configurations $t = \pm ir$ or $t = \pm r$ with $|t| = |r| = \frac{1}{2}$, respectively—that is, 25% of the incident energy is transmitted, 25% is reflected, and the amount of nonradiative losses on the beam splitters is 50%. We fabricated two corresponding beam splitters designated samples I and II, respectively. The features of each beam splitter are reported in Table 1. We characterized the phase difference between r and t by an interferometric method. We used the plasmonic beam splitter as the output beam splitter of a Mach-Zehnder interferometer. We split an 806-nm continuous-wave laser beam in this interferometer and recorded the interference fringes at both output ports of the setup when increasing the relative delay δ_{HOM}. We then measured the average phase difference between the two signals that were recorded on the two output channels to get ϕ_{rt}.

Figure 3 is a plot of the coincidence rate with respect to the HOM delay δ_{HOM} between both arms when sample I was used. The inset is a plot of the sinusoidal fringes obtained at the outputs of the beam splitter when illuminating with a laser at 806 nm. It is seen that the fringes are in phase opposition, confirming the ±90° phase shift between r and t. The plot displays an HOM-like dip, with a 61% contrast, unambiguously in the quantum regime beyond the 50% limit (33). This result is analogous to the coalescence effect observed in two-photon quantum interference on a lossless beam splitter and confirms the bosonic behavior of a single plasmon, here achieved with freely propagating, nonguided SPPs on a gold surface.

We then move to the next beam splitter, sample II. The inset of Fig. 4 shows that classical fringes at the output are in phase. In this case, orthogonality is not preserved between output modes of the SPBS. The two-particle quantum interference experiment is now characterized by an HOM peak, an increase in coincidence rate with respect to the classical case. The contrast is around 70%, again in a clear quantum regime. The peak illustrates that when combining on this beam splitter, SPPs tend to emerge from two different outputs. This anti-coalescence effect highlights the fundamental role of the SPBS in quantum interference.

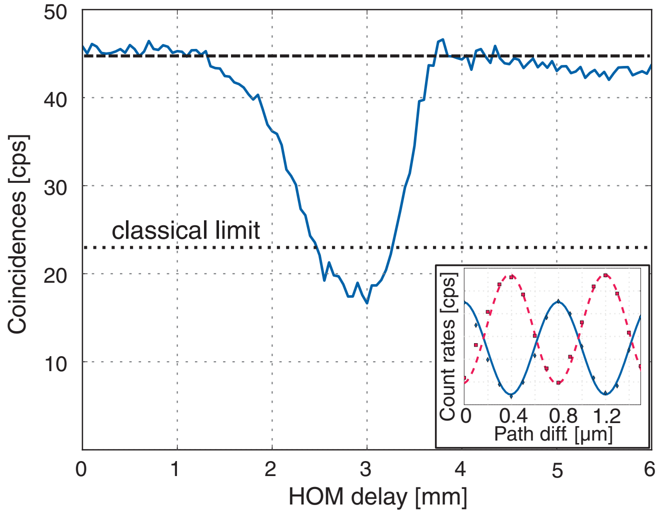

Fig. 3. Observation of a plasmonic Hong-Ou-Mandel coalescence effect with freely propagating single SPPs on sample I. The plot displays the coincidence count rates with respect to the HOM delay δ_{HOM} between both particles. The delay is indicated as a relative measurement starting from the initial position of the optical apparatus. The coincidence counts have been recorded every 50 μm, with a 5-min integration time, which is long enough to limit uncertainty on the count rate below 1 coincidence per second (cps). The contrast of the dip is ~61 ± 2%, above the quantum limit at 50%. The black dashed line at the top of the graph is the baseline of the dip profile. It represents the expected level of coincidences for independent particles. The inset displays short interferograms of the classical fringes recorded by SPCMs A (red dashed line and squares) and B (blue line and diamonds). Similar to the lossless configuration, the observed sine waves are in phase opposition. Path diff., path difference.

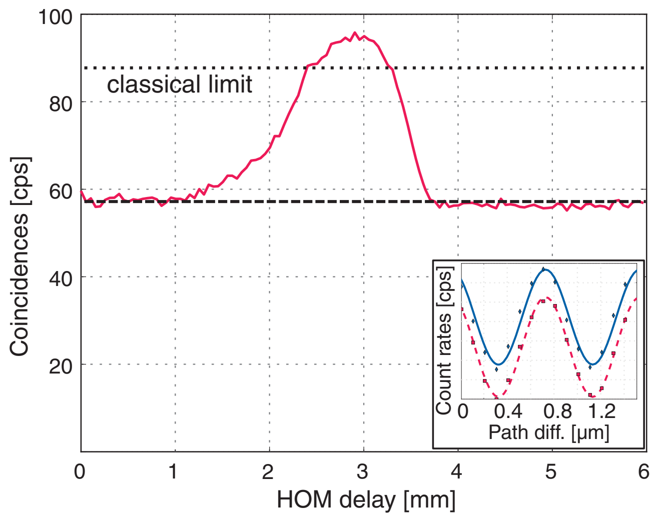

Fig. 4. Observation of a plasmonic Hong-Ou-Mandel peak when using sample II. We plotted the coincidence count rate between SPCMs A and B for a varying delay between the particles interfering on the SPBS and under the same experimental conditions as previously used. The contrast of the peak is 70 ± 2%. Here, the SPBS coefficients have been chosen so that the classical sine fringes recorded by SPCM A (red dashed line and squares) and SPCM B (blue line and diamonds) are in phase (**inset**). The black dashed line is a baseline for the peak profile. This observation can be interpreted as an anti-coalescence effect.

We have observed experimentally the coalescence of surface plasmons at a lossy beam splitter when $t = \pm ir$, thereby reproducing the results expected for bosons with a lossless beam splitter. However, in the particular case $t = \pm r$ with $|t| = |r| = \frac{1}{2}$, we have shown that the dip is converted into an anti-coalescence peak. This feature is usually associated with fermions when using nonlossy beam splitters (16) because there cannot be two fermions in the same output path. Although our experiment exhibits a correlation peak, it differs from previous observations of boson anti-coalescence with antisymmetric states mimicking fermions (17, 18). We have derived the output states repartition for both situations (33), and it is shown that they are different. Another interesting consequence of the particular phase of the SPBS predicted in (23) is nonlinear absorption: That is, only two photons or none can be absorbed, so that the probability of observing a single photon is zero.

The observation of a correlation peak that is not related to a fermionic behavior raises the question of the effect of a lossy beam splitter in the fermionic case. We show in (33) that the phase property of the SPBS converts the usual fermionic correlation peak into a correlation dip. The dip corresponds to no particle in one path resulting from interference, and the absorption of one particle, required by the Pauli exclusion principle. Hence, we find that one and only one fermion is always absorbed, at odds with the bosonic nonlinear absorption. This quantum coherent absorption of fermions is reminiscent of the (classical) coherent total absorption for photons (25, 34). To observe this effect, we may use two photons in a product state of a polarization antisymmetric Bell state and a spatial antisymmetric state that mimics a fermionic state. We predict an output with one photon in one arm and one photon absorbed (33), in marked contrast with the bosonic case where this probability was zero.

The results of our study illustrate that the output of a beam splitter illuminated by two particles depends not only on their quantum nature but also on the symmetry of the spatial part of the two-particle state and on the phase of the beam splitter reflection and transmission factors. As previously shown (*23*, *24*), the presence of losses adds a new degree of freedom in the quantum systems.

REFERENCES AND NOTES

1. R. H. Ritchie, *Phys. Rev.* **106**, 874–881 (1957).
2. A. V. Akimov *et al.*, *Nature* **450**, 402–406 (2007).
3. Y.-J. Cai *et al.*, *Phys. Rev. Appl.* **2**, 014004 (2014).
4. R. Kolesov *et al.*, *Nat. Phys.* **5**, 470–474 (2009).
5. M.-C. Dheur *et al.*, *Sci. Adv.* **2**, e1501574 (2016).
6. E. Altewischer, M. P. van Exter, J. P. Woerdman, *Nature* **418**, 304–306 (2002).
7. S. Fasel *et al.*, *Phys. Rev. Lett.* **94**, 110501 (2005).
8. X. F. Ren, G. P. Guo, Y. F. Huang, C. F. Li, G. C. Guo, *EPL* **76**, 753–759 (2006).
9. R. W. Heeres, L. P. Kouwenhoven, V. Zwiller, *Nat. Nanotechnol.* **8**, 719–722 (2013).
10. J. S. Fakonas, H. Lee, Y. A. Kelaita, H. A. Atwater, *Nat. Photonics* **8**, 317–320 (2014).
11. S. D. Gupta, G. S. Agarwal, *Opt. Lett.* **39**, 390–393 (2014).
12. G. Di Martino *et al.*, *Phys. Rev. Appl.* **1**, 034004 (2014).
13. S. M. Wang *et al.*, *Nat. Commun.* **7**, 11490 (2016).
14. E. Knill, R. Laflamme, G. J. Milburn, *Nature* **409**, 46–52 (2001).
15. D. E. Chang, A. S. Sørensen, P. R. Hemmer, M. D. Lukin, *Phys. Rev. Lett.* **97**, 053002 (2006).
16. R. Loudon, *Phys. Rev. A* **58**, 4904–4909 (1998).
17. A. Zeilinger, *Phys. Scr.* **T76**, 203–209 (1998).
18. M. Michler, K. Mattle, H. Weinfurter, A. Zeilinger, *Phys. Rev. A* **53**, R1209–R1212 (1996).
19. J. C. F. Matthews *et al.*, *Sci. Rep.* **3**, 1539 (2013).
20. H. Defienne, M. Barbieri, I. A. Walmsley, B. J. Smith, S. Gigan, *Sci. Adv.* **2**, e1501054 (2016).
21. T. A. W. Wolterink *et al.*, *Phys. Rev. A* **93**, 053817 (2016).
22. P. G. Kwiat, A. M. Steinberg, R. Y. Chiao, *Phys. Rev. A* **45**, 7729–7739 (1992).
23. S. M. Barnett, J. Jeffers, A. Gatti, R. Loudon, *Phys. Rev. A* **57**, 2134–2145 (1998).
24. J. Jeffers, *J. Mod. Opt.* **47**, 1819–1824 (2000).
25. T. Roger *et al.*, *Nat. Commun.* **6**, 7031 (2015).
26. T. Roger *et al.*, *Phys. Rev. Lett.* **117**, 023601 (2016).
27. C. K. Hong, Z. Y. Ou, L. Mandel, *Phys. Rev. Lett.* **59**, 2044–2046 (1987).
28. A. Zeilinger, H. J. Bernstein, M. A. Horne, *J. Mod. Opt.* **41**, 2375–2384 (1994).
29. M. S. Tame *et al.*, *Phys. Rev. Lett.* **101**, 190504 (2008).
30. A. Baron *et al.*, *Nano Lett.* **11**, 4207–4212 (2011).
31. M. U. González *et al.*, *Phys. Rev. B* **73**, 155416 (2006).
32. E. Silberstein, P. Lalanne, J.-P. Hugonin, Q. Cao, *JOSA A* **18**, 2865–2875 (2001).
33. Materials and methods and further calculations are available as supplementary materials.
34. W. Wan *et al.*, *Science* **331**, 889–892 (2011).

ACKNOWLEDGMENTS

We are grateful to T. W. Ebbesen, P. Lalanne, and J.-C. Rodier for their crucial role in this project. We also acknowledge F. Cadiz and N. Schilder for their help in the beginning of this study, as well as L. Jacubowiez, A. Browaeys, C. Westbrook, and P. Grangier for fruitful discussions. The research was supported by a DGA-MRIS (Direction Générale de l'Armement, Mission Recherche et Innovation Scientifique) scholarship, by RTRA (Réseau Thématique de Recherche Avancée) Triangle de la Physique, by the SAFRAN-IOGS chair on Ultimate Photonics, and by a public grant overseen by the French National Research Agency (ANR) as part of the "Investissements d'Avenir" program (reference: ANR-10-LABX-0035, Labex NanoSaclay). J.-J.G. acknowledges the support of Institut Universitaire de France. All data needed to evaluate the conclusions in this study are presented in the paper and/or in the supplementary materials. Additional data related to this study may be requested from F.M. (francois.marquier@institutoptique.fr).

SUPPLEMENTARY MATERIALS

www.sciencemag.org/content/356/6345/1373/suppl/DC1
Materials and Methods
Supplementary Text
Reference (*35*)

8 February 2017; accepted 11 May 2017
Published online 25 May 2017
10.1126/science.aam9353

Science

Anti-coalescence of bosons on a lossy beam splitter

Benjamin Vest, Marie-Christine Dheur, Éloïse Devaux, Alexandre Baron, Emmanuel Rousseau, Jean-Paul Hugonin, Jean-Jacques Greffet, Gaétan Messin and François Marquier

Science **356** (6345), 1373-1376.
DOI: 10.1126/science.aam9353originally published online May 25, 2017

To bunch or to antibunch

Particles of matter can be classed as either as bosons or fermions. Their subsequent behavior in terms of their physical properties and interactions depends on which quantum statistics they obey. Photons, for instance, are bosons and tend to bunch. Electrons are fermions and tend to antibunch. Vest *et al.* show that surface plasmon polaritons, a hybrid excitation of light and electrons, can exhibit both kinds of behavior (see the Perspective by Faccio). By tuning the level of loss in their system, bunching and antibunching of interfering plasmons can be seen.

Science, this issue p. 1373; see also p. 1336